STEPS TOWARD DETERMINATION OF THE SIZE AND STRUCTURE OF THE BROAD-LINE REGION IN ACTIVE GALACTIC NUCLEI. VI. VARIABILITY OF NGC 3783 FROM GROUND-BASED DATA[1]

G. M. STIRPE,[2] C. WINGE,[3,4] B. ALTIERI,[5,6] D. ALLOIN,[7] E. L. AGUERO,[8,9] G. C. ANUPAMA,[10] R. ASHLEY,[11] R. BERTRAM,[12,13] J. H. CALDERON,[8] R. M. CATCHPOLE,[14] R. L. M. CORRADI,[5,15] E. COVINO,[16] H. A. DOTTORI,[3] M. W. FEAST,[11] K. K. GHOSH,[17] R. GIL HUTTON,[18,19] I. S. GLASS,[20] E. K. GREBEL,[5] L. JORDA,[5,7] C. KOEN,[20] C. D. LANEY,[20] M. MAIA,[21] F. MARANG,[20] Y. D. MAYYA,[22] N. MORRELL,[23] Y. NAKADA,[24] M. G. PASTORIZA,[3] A. K. PATI,[22] D. PELAT,[7] B. M. PETERSON,[12] T. P. PRABHU,[22] G. ROBERTS,[20] R. SAGAR,[22] I. SALAMANCA,[7] K. SEKIGUCHI,[20] T. STORCHI-BERGMANN,[3] A. SUBRAMANIAM,[22] H. VAN WINCKEL,[5,25] F. VAN WYK,[20] M. VILLADA,[8,9] R. M. WAGNER,[12,13] P. A. WHITELOCK,[20] H. WINKLER,[26] J. CLAVEL,[6] M. DIETRICH,[27] W. KOLLATSCHNY,[27] P. T. O'BRIEN,[28] G. C. PEROLA,[29] M. C. RECONDO-GONZÁLEZ,[30] P. RODRÍGUEZ-PASCUAL,[30] AND M. SANTOS-LLEÓ[7]

ABSTRACT

The Seyfert 1 galaxy NGC 3783 was intensely monitored in several bands between 1991 December and 1992 August. This paper presents the results from the ground-based observations in the optical and near-IR bands, which complement the data set formed by the *International Ultraviolet Explorer* (*IUE*) spectra, discussed elsewhere. Spectroscopic and photometric data from several observatories were combined in order to obtain well-sampled light curves of the continuum and of Hβ. During the campaign the source underwent significant variability. The light curves of the optical continuum and of Hβ display strong similarities to those obtained with the *IUE*. The near-IR flux did not vary significantly except for a slight increase at the end of the campaign.

The cross-correlation analysis shows that the variations of the optical continuum have a lag of 1 day or less with respect to those of the UV continuum, with an uncertainty of ≤ 4 days. The integrated flux of Hβ varies with a delay of about 8 days. These results confirm that (1) the continuum variations occur simultaneously or with a very small lag across the entire UV-optical range, as in the Seyfert galaxy NGC 5548; and (2) the emission lines of NGC 3783 respond to ionizing continuum variations with less delay than those of NGC 5548. As observed in NGC 5548, the lag of Hβ with respect to the continuum is greater than those of the high-ionization lines.

Subject headings: galaxies: active — galaxies: individual (NGC 3783) — galaxies: nuclei — galaxies: photometry — galaxies: Seyfert

[1] Partly based on observations collected at the European Southern Observatory, La Silla, Chile.

[2] Osservatorio Astronomico di Bologna, Via Zamboni 33, 40126 Bologna, Italy; stirpe@alma02.bo.astro.it.

[3] Departamento de Astronomia, Instituto de Física, Universidade Federal do Rio Grande do Sul, Avenida Bento Gonçalves, 9500, CP15051, CEP 91500, Porto Alegre, RS, Brazil.

[4] Visiting Astronomer at the Cerro Tololo Inter-American Observatory of the National Optical Observatories, operated by AURA, Inc., under contract with the National Science Foundation.

[5] European Southern Observatory, Casilla 19001, Santiago 19, Chile.

[6] ISO Observatory, ESA Astrophysics Division, ESTEC, Postbus 299, 2200 AG Noordwijk, The Netherlands.

[7] Observatoire de Paris, URA173 CNRS, Université Paris 7, Place Jules Janssen, 92195, Meudon Principal Cedex, France.

[8] Observatorio Astronómico de Córdoba, Córdoba, Argentina.

[9] Visiting Astronomer at the Complejo Astronómico El Leoncito (CASLEO), San Juan, Argentina.

[10] Inter-University Centre for Astronomy and Astrophysics, Post Bag 4, Ganeshkhind, Pune 411007, India.

[11] Department of Astronomy, University of Cape Town, Private Bag, 7700 Rondebosch, Cape Town, South Africa.

[12] Department of Astronomy, The Ohio State University, 174 West 18th Avenue, Columbus, OH 43210.

[13] Postal address: Lowell Observatory, Mars Hill Road, 1400 West, Flagstaff, AZ 86001.

[14] Royal Greenwich Observatory, Madingley Road, Cambridge CB3 0HA, UK.

[15] Dipartimento di Astronomia, Università di Padova, Vicolo dell'Osservatorio 5, 35122 Padova, Italy.

[16] Osservatorio Astronomico di Capodimonte, Via Moiariello 16, 80131 Napoli, Italy.

[17] Vainu Bappu Observatory, Indian Institute of Astrophysics, Kavalur, Alangayam 635701, Tamil Nadu, India.

[18] Observatorio Astronómico Felix Aguilar, San Juan, Argentina.

[19] Yale Southern Observatory, San Juan, Argentina.

[20] South African Astronomical Observatory, P.O. Box 9, Observatory 7935, Cape Town, South Africa.

[21] Observatorio Nacional, CNPq, Rio de Janeiro, Brazil.

[22] Indian Institute of Astrophysics, Bangalore 560 034, India.

[23] Observatorio Astronómico de La Plata, La Plata, Argentina.

[24] Kiso Observatory, Institute of Astronomy, University of Tokyo, Japan.

[25] Astronomisch Instituut, Katholieke Universiteit Leuven, Celestijnenlaan 200 B, 3001 Heverlee, Belgium.

[26] Department of Physics, Vista University, Soweto Campus, Private Bag X09, 2013 Bertsham, Johannesburg, South Africa.

[27] Universitäts-Sternwarte, Geismarlandstraße 11, W-3400 Göttingen, Germany.

[28] Department of Physics and Astronomy, UCL, Gower Street, London WC1E 6BT, UK.

[29] Istituto Astronomico dell'Università, Via Lancisi 29, 00161 Roma, Italy.

[30] ESA *IUE* Observatory, P.O. Box 50727, 28080 Madrid, Spain.

1. INTRODUCTION

The nucleus of the Seyfert 1 galaxy NGC 3783 ($\alpha_{1950.0} = 11^h36^m33^s.0$, $\delta_{1950.0} = 37°27'41''$; $z = 0.0097$; $m_V \sim 13$) is one of the brightest and therefore best-studied active galactic nuclei (AGNs) of the southern hemisphere. The optical spectrum of this source, which has been extensively studied by Pelat, Alloin, & Fosbury (1981) and Evans (1988), presents very strong emission lines, with a high degree of ionization (Fig. 1). Variations of the broad components of the optical emission lines have been reported by Menzies & Feast (1983), Stirpe, de Bruyn, & van Groningen (1988), Evans (1989), Winge, Pastoriza, & Storchi-Bergmann (1990), Winge et al. (1992), and Winkler (1992). De Ruiter & Lub (1986) and Winkler et al. (1992) present multiband photometric observations, which show that the source has varied by several tenths of a magnitude. Photometric U data shown by Glass (1992) display variations in excess of 1.1 mag. Variations have also been observed in the near-IR by Glass (1992), from ~ 0.5 mag at J (1.25 μm) to ~ 1.1 mag at L (3.5 μm).

Because of this history of variability, NGC 3783 was judged a suitable candidate for an intensive monitoring campaign, similar to that carried out on NGC 5548 by the International AGN Watch consortium (Clavel et al. 1991, Peterson et al. 1991, 1992, Dietrich et al. 1993, and Peterson et al. 1994, hereafter Papers I–IV and VII, respectively; Maoz et al. 1993; see also the review by Peterson 1993). The monitoring of NGC 3783 took place between 1991 December and 1992 August, and made use of the *International Ultraviolet Explorer* (*IUE*) and of several ground-based telescopes, mainly in the southern hemisphere. The results of the *IUE* observations are presented by Reichert et al. (1994, hereafter Paper V). This paper presents the first results from the ground-based spectroscopic and photometric observations in the optical and near-IR bands. Section 2 gives a description of the observations, § 3 describes how the spectra were corrected for slit losses, §§ 4 and 5 describe how the light curves of the continuum and of Hβ were obtained, § 6 presents a discussion and analysis of the light curves, and § 7 summarizes our main conclusions.

2. OBSERVATIONS

2.1. *Spectroscopy*

Spectroscopic observations were obtained at Cerro Tololo Inter-American Observatory (CTIO) in Chile; at the European Southern Observatory (ESO), La Silla, Chile; at the Complejo Astronómico El Leoncito (CASLEO), Argentina; at the Ohio State University (OSU) Perkins reflector at Lowell Obsevatory; and at Vainu Bappu Observatory, Kavalur, India. All spectra were recorded on CCDs, with the exception of those taken at the CTIO 1 m telescope, where the 2D-FRUTTI detector was used. The bulk of the data comes from this telescope and from the ESO 1.5 m telescope: the CTIO spectra were all obtained with the same instrumental setup, and therefore form a very homogeneous data set; the ESO spectra vary widely in resolution and wavelength coverage, because the program shared nights with other scheduled observers, who had priority in the choice of the grating. A journal of the observations is given in Table 1: the columns list respectively the Julian Date minus 2,440,000 and the UT date at the midpoint of the integration, a code (A–E) which indicates where the spectrum was obtained, the air mass at the midpoint of the integration, the area of the aperture (slit width × length) in square arcseconds, the resolution and wavelength range in

angstroms, and the integration times in seconds. The seeing was generally between 1'' and 2''. Epochs with subarcsecond seeing include JD 2,448,609, JD 2,448,649, and JD 2,448,824. Bad seeing ($\sim 3''$) was recorded on JD 2,448,820.

All spectra were reduced using standard techniques. This paper presents the light curve of the optical continuum and Hβ only; the analysis of other emission lines will be presented in a future paper. Unless otherwise stated, all wavelengths quoted in this paper are in the observed frame.

2.2. *Optical Photometry*

Photoelectric $UBV(RI)_C$ photometry was obtained at the 0.5 m telescope of the South African Astronomical Observatory at Sutherland, using the SAAO photometer equipped with a Hamamatsu GaAs photomultiplier tube. An aperture of 20'' in diameter was used. The seeing varied between 1'' and 5''. The observations and reduction were performed as described in Winkler et al. (1992). The results are listed in Table 2. The uncertainties on the magnitudes are 0.03 mag.

Photoelectric UBV photometry was obtained at the 0.7 m Charles D. Perrin telescope at the Observatorio Astronómico Felix Aguilar (OAFA), San Juan, Argentina, through an aperture of 33'' in diameter. The photometer was equipped with an RCA 31034A photomultiplier tube. The seeing was between 2'' and 3'' at all epochs. The data were calibrated using standard star fluxes from Landolt (1973, 1983). The measurements are listed in Table 3. The first part of the campaign was affected by the presence in the atmosphere of dust from the Hudson volcano, which caused some color measurements to be unreliable: these have been omitted from the table. The uncertainties on the magnitudes are 0.03 mag.

CCD photometry in BVR was obtained at the 1 m telescope of the Vainu Bappu Observatory (VBO). The seeing was between 2'' and 3'' for all observations. Bias subtraction and flat-fielding was performed on the frames, using Starlink routines. The flux of NGC 3783 was measured with circular apertures with a diameter of 18'', and calibrated with the nearby star SAO 202668, exposed on the same frames. The results are listed in Table 4. The uncertainties are 0.05 mag for the magnitudes, and 0.03 mag for the colors.

There is a systematic difference between $B-V$ values obtained at SAAO and VBO on close dates, which cannot be accounted for entirely by the slightly different apertures used. Given the peculiar shape of AGN spectra, it is likely that the difference is caused by the large color term required to convert the observed VBO values to the Johnson photometric system. The accuracies quoted do not take this systematic effect into account, but are correct within the individual data sets.

2.3. *Infrared Photometry*

$JHKL$ photometry was obtained at SAAO, through a 12'' aperture, using the Mk III infrared photometer attached to the 1.9 m telescope. The observations and reduction took place as described by Glass (1992). The chopping distance was 30'' north and south of the nucleus. Tests with larger chopping distances were made on NGC 3783 in 1988 March: a distance of 60'' yielded fluxes which differed by at most 0.01 mag from those obtained with the 30'' distance. Therefore, the latter was considered sufficient.

The fluxes were calibrated in the SAAO standard system (Carter 1990), using the standard star HR 4523. Other standards observed during the same nights provided a check on the photometric accuracy. The magnitudes are given in Table 5.

TABLE 1

JOURNAL OF SPECTROSCOPIC OBSERVATIONS

JD −2,440,000	UT Date	Origin	Air Mass	Aperture (arcsec × arcsec)	Resolution (Å)	Range (Å)	Integration Time (s)
8593.83	1991 Dec 3	D	1.36	3 × 3.3	15	3800–9000	1800
8597.81	1991 Dec 7	D	1.38	3 × 3.3	2	5050–7095	3600
8605.83	1991 Dec 15	D	1.22	3 × 3.3	4	3770–9000	2400
8607.83	1991 Dec 17	A	1.15	5 × 10	8	3515–7060	2500
8609.81	1991 Dec 19	D	1.24	3 × 3.3	4	3600–7300	3600
8613.84	1991 Dec 23	D′	1.12	2 × 3.3	6	4455–7100	2400
8621.83	1991 Dec 31	D	1.12	3 × 3.3	7	3690–9000	4200
8623.83	1992 Jan 2	A	1.06	5 × 10	8	3570–7105	2700
8625.81	1992 Jan 4	D	1.10	3 × 3.3	8	5700–9000	3600
8627.83	1992 Jan 6	A	1.05	5 × 10	8	3540–7085	3300
8631.84	1992 Jan 10	A	1.02	5 × 10	8	3555–7090	2400
8633.74	1992 Jan 12	C	1.28	6.6 × 16	8	3615–5755	5400
8633.81	1992 Jan 12	D	1.06	3 × 3.3	4	4000–6920	3600
8635.83	1992 Jan 14	A	1.02	5 × 10	8	3545–7095	3000
8637.78	1992 Jan 16	C	1.10	6.6 × 16	8	3720–5685	1800
8638.75	1992 Jan 17	C	1.16	6.6 × 16	8	3705–5670	1800
8639.84	1992 Jan 18	A	1.01	5 × 10	8	3565–7100	2700
8642.78	1992 Jan 21	C	1.06	6.6 × 16	8	3800–5795	1800
8643.72	1992 Jan 22	A	1.26	5 × 10	8	3565–7115	3600
8645.82	1992 Jan 24	D	1.02	3 × 3.3	6	3500–8960	3600
8647.76	1992 Jan 26	A	1.07	5 × 10	8	3565–7110	3600
8649.83	1992 Jan 28	D	1.01	3 × 3.3	2	4265–6265	3600
8651.76	1992 Jan 30	A	1.06	5 × 10	8	3680–7230	3600
8653.83	1992 Feb 1	D	1.02	3 × 3.3	4	4860–6850	4800
8656.77	1992 Feb 4	A	1.02	5 × 10	8	3675–7225	3600
8657.86	1992 Feb 5	D	1.17	3 × 3.3	6	3695–8855	3600
8660.77	1992 Feb 8	A	1.01	5 × 10	8	3670–7220	3600
8661.85	1992 Feb 9	D	1.08	3 × 3.3	6	3690–8855	3600
8664.77	1992 Feb 12	A	1.01	5 × 10	8	3670–7235	3600
8668.81	1992 Feb 16	A	1.02	5 × 10	8	3670–7230	3600
8672.72	1992 Feb 20	A	1.04	5 × 10	8	3640–7210	3600
8676.71	1992 Feb 24	A	1.04	5 × 10	8	3690–7240	3600
8677.80	1992 Feb 25	A	1.04	5 × 10	8	3665–7215	3600
8678.68	1992 Feb 26	A	1.08	5 × 10	8	3690–7235	3600
8681.71	1992 Feb 29	D	1.02	3 × 3.3	4	3540–7440	3600
8685.77	1992 Mar 4	D	1.05	3 × 3.3	6	3800–9200	3600
8685.80	1992 Mar 4	A′	1.08	5 × 10	8	3200–7410	60
8686.70	1992 Mar 5	C	1.01	6.6 × 16	8	3455–5500	1800
8687.74	1992 Mar 6	A″	1.01	5 × 10	12	3200–7730	480
8689.73	1992 Mar 8	D	1.02	3 × 3.3	4	3400–8060	3600
8689.80	1992 Mar 8	C	1.11	6.6 × 16	8	3600–5500	1800
8690.78	1992 Mar 9	C	1.07	6.6 × 16	8	3550–5600	1800
8694.31	1992 Mar 12	E	1.5	5.4 × 16	20	4020–7030	4500
8697.66	1992 Mar 16	D	1.02	3 × 3.3	4	5650–8490	3600
8704.58	1992 Mar 23	A	1.17	5 × 10	8	3665–7215	3600
8705.67	1992 Mar 24	D	1.02	3 × 3.3	3	6060–8455	3600
8710.67	1992 Mar 29	D	1.01	3 × 3.3	2	4050–6020	3600
8712.59	1992 Mar 31	A	1.07	5 × 10	8	3655–7205	3600
8715.63	1992 Apr 3	D	1.01	3 × 3.3	2	4880–6870	3600
8716.60	1992 Apr 4	A	1.04	5 × 10	8	3645–7210	3600
8720.59	1992 Apr 8	A	1.03	5 × 10	8	3660–7225	3600
8724.56	1992 Apr 12	A	1.06	5 × 10	8	3670–7220	3600
8728.55	1992 Apr 16	A	1.06	5 × 10	8	3660–7215	3600
8732.56	1992 Apr 20	A	1.03	5 × 10	8	3640–7190	3600
8736.55	1992 Apr 24	A	1.02	5 × 10	8	3665–7215	3600
8737.55	1992 Apr 25	D	1.03	3 × 3.3	4	3850–7580	3600
8742.67	1992 Apr 30	B	3.38	5 × 7.5	8	4510–5670	1200
8744.61	1992 May 2	A	1.05	5 × 10	8	3630–7185	3600
8745.49	1992 May 3	D	1.08	3 × 3.3	2	4950–6900	2400
8749.52	1992 May 7	D	1.03	3 × 3.3	3	4300–6900	3600
8752.57	1992 May 10	A	1.03	5 × 10	8	3650–7210	3600
8753.54	1992 May 11	D	1.01	3 × 3.3	3	4500–6895	3600
8764.56	1992 May 22	A	1.10	5 × 10	8	3645–7195	3600
8765.52	1992 May 23	D	1.02	3 × 3.3	2	4950–6800	2400
8772.63	1992 May 30	A	1.34	5 × 10	8	3695–7240	3600
8773.51	1992 May 31	D	1.02	3 × 3.3	3	5200–7455	3600
8776.56	1992 Jun 3	A	1.10	5 × 10	8	3675–7225	3600
8777.49	1992 Jun 3	D	1.02	3 × 3.3	6	3200–8000	3600
8794.57	1992 Jun 21	A	1.35	5 × 10	8	3660–7210	3600
8800.52	1992 Jun 27	D	1.20	3 × 3.3	1	4105–5095	3600
8802.5	1992 Jun 29	D	1.2	3 × 3.3	4	4750–8200	3600
8803.5	1992 Jun 30	D	1.2	3 × 3.3	4	4750–8200	3600
8804.47	1992 Jun 30	A	1.08	5 × 10	8	3630–7185	3600

TABLE 1—*Continued*

JD −2,440,000	UT Date	Origin	Air Mass	Aperture (arcsec × arcsec)	Resolution (Å)	Range (Å)	Integration Time (s)
8805.5	1992 Jul 2	D	1.2	3 × 3.3	15	3400–8400	3600
8806.57	1992 Jul 3	A	1.58	5 × 10	8	3600–7150	3600
8808.47	1992 Jul 4	A	1.10	5 × 10	8	3590–7140	3600
8820.55	1992 Jul 17	D	1.96	3 × 3.3	4	3700–7000	1200
8822.48	1992 Jul 18	A	1.25	5 × 10	8	3590–7145	5400
8822.53	1992 Jul 19	D	1.61	3 × 3.3	4	3700–7000	4500
8823.50	1992 Jul 20	D	>2	3 × 3.3	4	3700–7000	3600
8824.47	1992 Jul 20	A	1.23	5 × 10	8	3590–7140	5400
8824.52	1992 Jul 21	D	1.6	3 × 3.3	4	3700–7000	1800
8826.47	1992 Jul 22	A	1.25	5 × 10	8	3590–7140	1800
8830.48	1992 Jul 26	A	1.31	5 × 10	8	3645–7195	5400
8832.46	1992 Jul 28	A	1.32	5 × 10	8	3645–7195	5400
8841.49	1992 Aug 6	D	1.76	3 × 3.3	6	4600–8000	3600
8844.50	1992 Aug 9	D	1.83	3 × 3.3	6	4600–8200	3600

NOTE.—Codes for data origin: A—1.0 m CTIO telescope + spectrograph + 2D FRUTTI; A'—4.0 m CTIO telescope + Ritchey-Chrétien spectrograph + CCD; A″—1.5 m CTIO telescope + spectrograph + CCD; B—1.8 m Perkins telescope + Ohio State spectrograph + CCD; C—2.2 m CASLEO telescope + Boller & Chivens spectrograph + CCD; D—1.5 m ESO spectroscopic telescope + Boller & Chivens spectrograph + CCD; D'—2.2 m ESO/MPI telescope + EFOSC2 + CCD; E—1.0 m VBO telescope + Zeiss spectrograph + CCD.

TABLE 2

PHOTOELECTRIC PHOTOMETRY FROM SAAO (20″ aperture)

JD −2,440,000	V	B−V	U−B	V−R_C	V−I_C
8610.56.........	12.93	0.63	−0.67	0.53	1.00
8622.55.........	12.96	0.61	−0.65	0.56	1.02
8630.57.........	12.96	0.66	−0.60	0.55	1.04
8634.55.........	12.98	0.65	−0.60	0.56	1.03
8638.57.........	12.96	0.65	−0.63	0.57	1.04
8644.56.........	12.94	0.60	−0.65	0.56	1.02
8651.58.........	12.94	0.63	−0.66	0.55	1.02
8655.58.........	12.93	0.60	−0.68	0.55	1.03
8659.54.........	12.92	0.60	−0.68	0.55	1.01
8663.53.........	12.93	0.62	−0.66	0.57	1.04
8671.52.........	12.98	0.61	−0.59	0.56	1.03
8684.52.........	13.00	0.67	−0.60	0.57	1.05
8688.60.........	13.11	0.68	−0.58	0.58	1.07
8700.45.........	13.05	0.72	−0.55	0.58	1.06
8704.42.........	13.08	0.70	−0.57	0.58	1.09
8714.41.........	13.03	0.63	−0.65	0.55	1.02
8717.50.........	12.99	0.64	−0.63	0.54	1.03
8729.38.........	12.97	0.63	−0.65	0.56	1.04
8733.36.........	12.97	0.63	−0.64	0.56	1.02
8743.40.........	12.96	0.65	−0.63	0.55	1.03
8747.34.........	12.96	0.63	−0.64	0.55	1.04
8802.25.........	12.96	0.60	−0.65	0.56	1.03
8803.27.........	12.92	0.61	−0.66	0.54	1.00
8823.22.........	12.91	0.62	−0.65	0.51	1.02

TABLE 3

PHOTOELECTRIC PHOTOMETRY FROM OAFA (33″ aperture)

JD −2,440,000	V	B−V	U−B
8638.69.........	12.64	...	...
8653.73.........	12.67	...	...
8653.75.........	12.68	...	...
8661.75.........	12.65	...	...
8663.69.........	12.67	0.71	...
8665.76.........	12.69	0.72	−0.70
8665.77.........	12.68	0.70	−0.60
8690.65.........	12.72	0.71	−0.50
8716.66.........	12.68	0.68	−0.54
8743.54.........	12.70	0.69	−0.48
8809.54.........	12.61	0.66	−0.61
8833.52.........	12.60	0.63	−0.56

TABLE 4

CCD PHOTOMETRY FROM VBO (18″ aperture)

JD −2,440,000	V	B−V	V−R
8657.41.........	13.00	0.51	0.63
8657.44.........	12.98	0.51	0.63
8688.31.........	13.13	0.63	0.68
8689.31.........	13.13	0.61	0.67
8715.24.........	13.09	0.49	0.65

TABLE 5

NEAR-IR OBSERVATIONS FROM SAAO (12″ aperture)

JD −2,440,000	J	H	K	L
8576..............	11.33	10.43	9.71	8.32 ± 0.06
8593..............	11.41	10.52	9.76	8.37 ± 0.11
8629..............	11.33	10.44	9.70	8.40 ± 0.05
8630..............	11.37	10.44	9.71	8.35 ± 0.06
8632..............	11.33	10.44	9.70	8.32 ± 0.06
8633..............	11.35	10.43	9.70	8.34 ± 0.06
8634..............	11.34	10.45	9.71	8.37 ± 0.05
8671..............	11.35	10.46	9.69	8.34 ± 0.06
8674..............	11.32	10.42	9.67	8.29 ± 0.06
8675..............	11.32	10.41	9.65	8.23 ± 0.06
8700..............	11.40	10.45	9.70	8.39 ± 0.06
8727..............	11.33	10.43	9.69	8.34 ± 0.05
8731..............	11.34	10.45	9.72	8.31 ± 0.06
8733..............	11.35	10.43	9.69	8.38 ± 0.06
8734..............	11.33	10.45	9.70	8.39 ± 0.06
8735..............	11.24	10.44	9.72	8.30 ± 0.06
8768..............	11.28	10.47	9.72	8.36 ± 0.05
8783..............	11.17	10.39	9.65	8.31 ± 0.06
8786..............	11.09	10.27	9.62	8.32 ± 0.06
8789..............	11.16	10.34	9.60	8.32 ± 0.08
8790..............	11.07	10.27	9.58	8.24 ± 0.06
8792..............	11.16	10.35	9.63	8.27 ± 0.06
8804..............	11.13	10.29	9.59	8.22 ± 0.05
8834..............	11.20	10.35	9.60	8.26 ± 0.05

The uncertainty of the J, H, and K magnitudes is 0.03 at all epochs. The uncertainties of the L magnitudes are listed in the table.

3. ABSOLUTE CALIBRATION OF THE SPECTRA

In order to correct for slit losses, the spectra which include $H\beta$ were internally calibrated relative to each other with the method described by van Groningen & Wanders (1992). The method finds the optimum scaling factor, wavelength shift, and convolution factor of one spectrum with respect to another one taken as reference, by slowly varying these parameters until the residuals of one or more constant narrow lines in the difference between the two spectra are minimized. One of the highest quality spectra (Fig. 1), obtained at ESO on 1991 December 18 (JD 2,448,609), was used as reference, and the residuals of the strong lines [O III] $\lambda\lambda4959$, 5007 were minimized. More than 90% of the multiplicative scaling factors yielded by the scaling program are between 0.8 and 1.5. The accuracy of the internal calibration is $\sim 2\%$ for most of the spectra, judging from the [O III] residuals obtained when slightly varying the scaling factor. Although the ESO spectra were obtained through a considerably narrower slit, differential light losses caused by the slightly extended [O III] emission (Winge et al. 1992) were negligible: a comparison between subsets of ESO and CTIO line fluxes obtained with separations of 2 days at most showed that any systematic offset between the two data sets is less than 0.5%.

The accuracy of the internal calibration method for spectra of very different resolutions was tested by convolving some of the highest resolution spectra with a Gaussian of appropriate width, in order to simulate the lowest resolution used, and running the internal calibration program again: the resulting scaling factors differed from those obtained for the nonconvolved spectra by 3% at most, always in excess. This effect is partly compensated, when measuring the line flux (see § 5), by the fact that the lower resolution causes a small fraction of the flux to be lost at the edges of the integration interval: the resulting $H\beta$ flux, therefore, does not differ by more than 2%.

In order to obtain the absolute calibration of the spectra, the flux of [O III] $\lambda5007$ was measured in the five CTIO spectra in which the [O III] lines were strongest *before* the internal calibration: these spectra are of the best quality and presumably suffered the least from slit losses or bad observing conditions. The CTIO data set was chosen to obtain the absolute calibration because of its homogeneity and large aperture. The [O III] $\lambda5007$ measurements were obtained by fitting a straight pseudocontinuum under the line and integrating the flux above it. The fluxes are listed in Table 6, with their 1 σ uncertainties. The last line of the table gives the mean value and standard deviation of the listed values. We henceforth assume that the flux of [O III] $\lambda5007$ is 8.44×10^{-13} erg s^{-1} cm^{-2}. The [O III] $\lambda5007$ flux measured in the ESO spectrum used as reference for the internal calibration (JD 2,448,609) is 8.85×10^{-13} erg s^{-1} cm^{-2}: therefore, all internally calibrated spectra were multiplied by a factor of 0.95 in order to obtain the right absolute calibration.
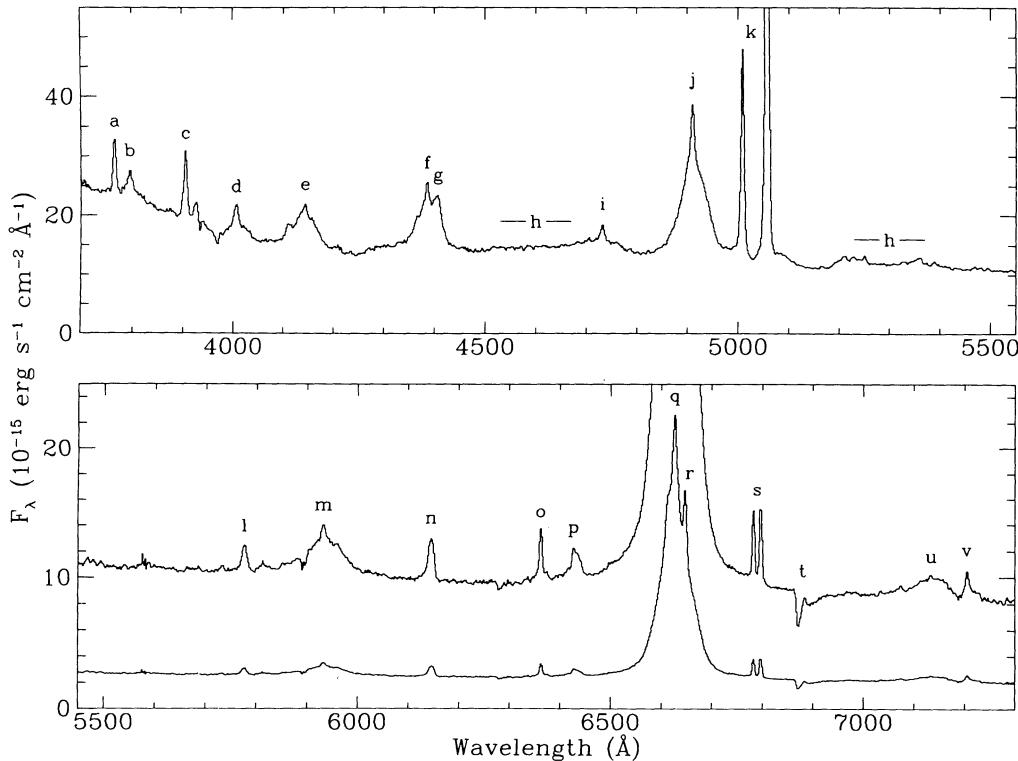

FIG. 1.—Spectrum of NGC 3783 obtained at ESO on 1991 December 18/19 (JD 2,448,609). The wavelength range was covered entirely by a single exposure, and is divided into two parts only for display purposes. The red part of the spectrum is shown at two different scales in order to display Hα in its entirety and to enhance the weaker lines. The scales in the lower panel differ by a factor of 4, and the vertical axis refers to the expanded scale. The letters indicate the main features as follows: a—[O II] $\lambda3727$; b—[Fe VII] $\lambda3760$; c—[Ne III] $\lambda3869$; d—[Ne III] $\lambda3968$; e—Hδ, f—Hγ; g—[O III] $\lambda4363$; h—Fe II multiplets; i—He II $\lambda4686$; j—Hβ; k—[O III] $\lambda\lambda4959$, 5007; l—[Fe VII] $\lambda5721$; m—He I $\lambda5876$; n—[Fe VII] $\lambda6086$; o—[O I] $\lambda6300$; p—[O I] $\lambda6363$ and [Fe X] $\lambda6375$; q—Hα; r—[N II] $\lambda6584$; s—[S II] $\lambda\lambda6717$, 6731; t—O₂ B band (telluric); u—He I $\lambda7065$; v—[Ar III] $\lambda7136$.

TABLE 6

ABSOLUTE FLUX OF [O III] λ5007

JD −2,440,000	Flux (10⁻¹³ erg s⁻¹ cm⁻²)
8607.............	8.44 ± 0.17
8651.............	8.36 ± 0.17
8678.............	8.52 ± 0.17
8716.............	8.39 ± 0.17
8724.............	8.46 ± 0.17
Mean............	8.435 ± 0.059

The value thus obtained for the [O III] λ5007 flux is about 15% less than the flux measured by Osmer, Smith, & Weedman (1974), and we will therefore assume that the systematic uncertainty of our absolute fluxes is of this order.

4. THE CONTINUUM LIGHT CURVES

4.1. Optical Continuum

The light curve of the optical continuum was obtained by combining spectral with photometric data. The continuum measurements must not be significantly contaminated by varying emission lines, which could introduce spurious delay in the continuum variations: care was taken, therefore, to use a part of the spectrum and a photometric band which are influenced as little as possible by the broad lines. For the spectra, an additional constraint is given by the necessity of obtaining the measurements in a region close to the [O III] lines, used as internal calibrators, so that inaccuracies in the response calibration do not introduce further uncertainties in the light curve.

The continuum flux was derived from the spectra by averaging the flux density in an interval of 20 Å centered at 5150 Å,

i.e., on the dip between the lines Fe II λλ5018 and 5169, which is considered to be the region close to Hβ least contaminated by emission lines (Fig. 2). Although the two Fe II lines may have slightly overlapping wings in this interval, their variations have a negligible influence on the continuum light curve.

The continuum measurements include a contribution from the underlying galaxy, which has a different spatial distribution than the nucleus: the galaxy has an apparent diameter of ∼2′, while the broad-line region (BLR) and the region which emits the nonstellar continuum are unresolved. Therefore, only the CTIO and OSU spectra were used, because of their similar large apertures: a wide slit, in fact, minimizes the differential light losses caused by the different spatial profiles of the nucleus and the underlying galaxy, and therefore ensures that the contribution of the stellar component to the continuum fluxes depends only weakly on the seeing value. Because the seeing was always lower than 2″ during the CTIO observations, the stellar component can be considered constant within the uncertainties.

The greatest source of uncertainty in the flux measurements is the internal calibration error, which in all spectra of good quality is considerably larger than the error introduced by the photon noise. Accordingly, most uncertainties were set at 2%. For some fluxes, obtained from spectra with lower signal-to-noise ratio, the error bars were set at 4%.

These points were then combined with the V fluxes, taken to represent measurements of the optical continuum: this band was chosen not only because its central wavelength is the closest to 5150 Å but also because it samples a section of the optical spectrum which is almost free from strong variable emission lines. The strongest broad lines are He I λ5876 and the Fe II blend centered at 5250 Å (rest wavelength). The equivalent widths of these features in the CTIO spectra are less than
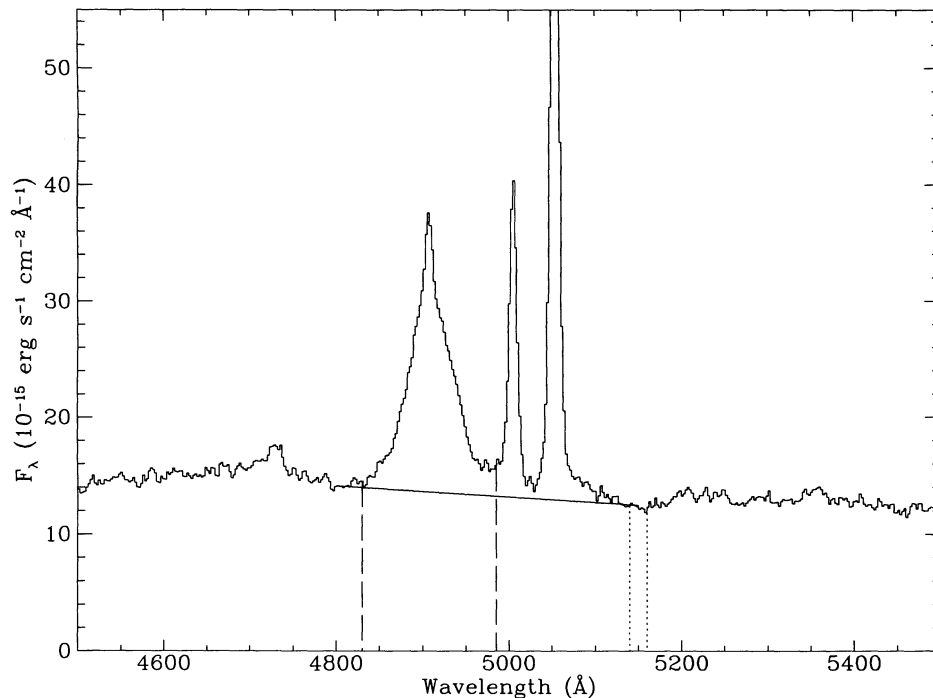

FIG. 2.—Hβ region of the spectrum obtained at CTIO on 1992 February 11/12 (JD 2,448,664). The straight lines illustrate the method used to measure the fluxes of Hβ and of the continuum: the continuous line indicates the straight-line fit which approximates the continuum under Hβ; the dashed lines indicate the limits of the line flux integration above the continuum fit; and the dotted lines indicate the limits of the interval used to average the continuum flux.

40 Å and less than 25 Å, respectively: we can therefore assume that the variations of these lines, and their possible delays with respect to those of the continuum, have a negligible effect on the V light curve. The main narrow lines present in the V band are [Fe VII] $\lambda5721$, which is weak, and the [O III] lines: the latter introduce at most only a slight constant offset in the V curve.

The V magnitudes were converted to flux densities using the relation

$$F_\lambda = 10^{(-0.4V - 8.47)} \qquad (1)$$

(Hayes & Latham 1975), with F_λ in erg s^{-1} cm^{-2} Å^{-1}. Although the spectrum of NGC 3783 does not have prominent emission features in the V band, this conversion may nevertheless be affected by a systematic error because of the differences between the spectrum of an AGN and that of the star (Vega) used to define relation (1). Furthermore, as explained in § 3, the spectroscopic continuum fluxes have a systematic uncertainty of 15%. For both these reasons the continuum flux densities obtained from different data sets were compared, before being combined in a single optical continuum curve, as follows.

If the conversion of the photometric V data to flux densities is correct, and if the absolute calibration of the spectroscopic fluxes is accurate, pairs of quasi-simultaneous fluxes from one of the photometric data sets and from the spectroscopic data set should align along a line of slope 1, and the photometric fluxes should have a positive offset caused by the underlying galaxy's higher contribution through the larger aperture. For each photometric data set, pairs formed by a photometric and a spectroscopic flux separated by at most 1 day are plotted in Figure 3. In each panel the continuous line is the line of slope 1 which best fits the data. For the first two subsets (SAAO versus spectroscopy and OAFA versus spectroscopy), two least-squares linear regression fits were calculated: ordinates against abscissae and vice versa. As shown in Figure 3, the slope of the bisector of the fits is close to unity for both subsets. Using the least-squares fit bisector to fine-tune the conversion would change the photometric fluxes by 1 σ at most. The fits were not calculated for the VBO versus spectroscopy subset, as it consists of only three points. Figure 3 shows that the relation between these points is also well represented by a line of slope 1.

This comparison of quasi-simultaneous pairs of points also allowed us to correct the photometric fluxes, in order to account for the different apertures used. The underlying galaxy contributes in different amounts to each data set. In particular, the photometric measurements, obtained through apertures with diameters of 18″, 20″, and 33″, are much higher than the spectroscopic fluxes, obtained through a 5″ × 10″ rectangular aperture. The comparison of quasi-simultaneous pairs of points yielded mean offsets of $(8.62 \pm 0.74) \times 10^{-15}$ erg s^{-1} cm^{-2} Å^{-1} for the VBO fluxes, $(9.71 \pm 0.66) \times 10^{-15}$ erg s^{-1} cm^{-2} Å^{-1} for the SAAO fluxes, and $(16.64 \pm 0.51) \times 10^{-15}$ erg s^{-1} cm^{-2} Å^{-1} for the OAFA fluxes. These quantities were subtracted from the photometric data, thus simulating photometry through a 5″ × 10″ rectangular aperture. The correction also automatically eliminates the constant offset which may be caused by the presence of the [O III] lines in the V band (see above). All fluxes are obviously still contaminated by stellar light from the underlying galaxy: given the large aperture, this component can be considered independent of seeing effects and therefore constant. As discussed in detail by Alloin et al. (1994), examination of the two-dimensional spectra made it possible
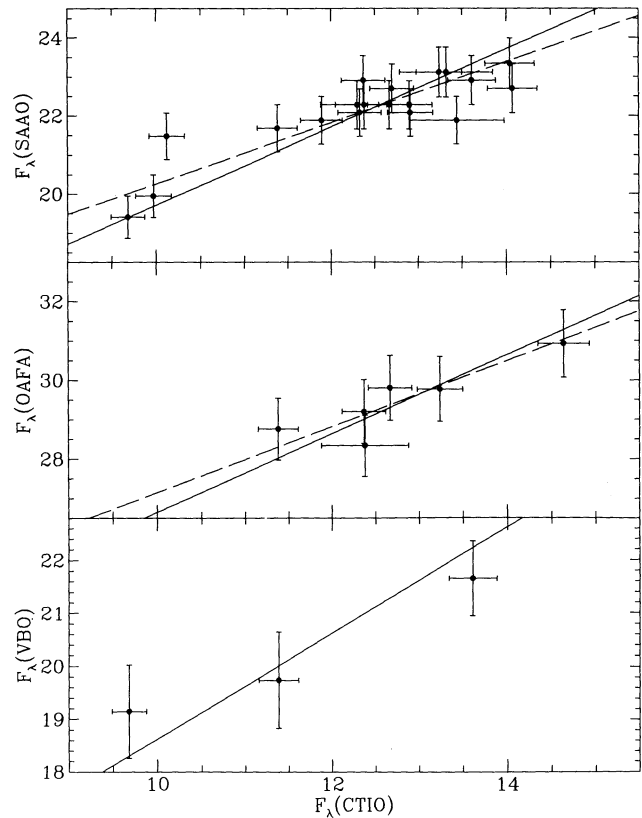

FIG. 3.—Comparison between quasi-simultaneous subsets of continuum fluxes obtained from the spectroscopic (CTIO) and photometric (SAAO, OAFA, and VBO) data sets. Units are 10^{-15} erg s^{-1} Å^{-1}. For each plotted point the corresponding observations were separated in time by 1 day at most. The photometric flux densities were obtained from the V data using equation (1). The solid lines have slope 1 and intercept the y-axis at the mean difference between ordinates and abscissae. This offset between different data sets is caused by the larger apertures used for the photometry, and therefore to a larger flux from the underlying galaxy. The dashed lines represent the bisectors of the least-squares linear regression fits calculated for ordinates against abscissae and vice versa.

to estimate that the stellar contribution is about 30% in the CTIO continuum measurements.

The continuum light curve obtained by combining the spectroscopic and photometric data is listed in Table 7 and plotted in Figure 4. Fluxes obtained at the same date were averaged and their uncertainties averaged quadratically. The median separation between consecutive points of the curve is 2.0 days. The variations of the optical continuum strongly resemble those of the UV continuum (Paper V).

4.2. Near-Infrared Continuum

Figure 5 shows the IR light curves obtained at SAAO: the magnitudes were converted to flux densities using the relations

$$F_\lambda(J) = 10^{(-0.4J - 9.54)}, \quad F_\lambda(K) = 10^{(-0.4K - 9.94)},$$

$$F_\lambda(H) = 10^{(-0.4H - 10.42)}, \quad F_\lambda(L) = 10^{(-0.4L - 11.16)},$$

with F_λ in erg s^{-1} cm^{-2} Å^{-1}. The IR flux showed little evidence for variation during the monitoring period and was generally lower than the long-term average in the K (2.2 μm) and L (3.5 μm) bands. The only significant change was an increase of $\sim 20\%$ at J, H, and K and $\sim 10\%$ at L between JD 2,448,768 and JD 2,448,790. The wavelength trend of this variation was

TABLE 7
OPTICAL CONTINUUM LIGHT CURVE

JD −2,440,000	F_λ(opt) (10^{-15} erg s^{-1} cm^{-2} Å^{-1})	Source	JD −2,440,000	F_λ(opt) (10^{-15} erg s^{-1} cm^{-2} Å^{-1})	Source
8607.83	13.02 ± 0.26	A	8690.65	11.06 ± 0.76	F
8610.56	14.19 ± 0.63	G	8700.45	10.79 ± 0.57	G
8622.55	12.57 ± 0.62	G	8704.50	10.00 ± 0.20	A, G
8623.83	12.90 ± 0.26	A	8712.59	11.78 ± 0.24	A
8627.83	12.35 ± 0.25	A	8714.41	11.18 ± 0.58	G
8630.57	12.57 ± 0.62	G	8715.24	11.11 ± 0.91	H
8631.84	12.30 ± 0.25	A	8716.60	11.44 ± 0.23	A, F
8634.55	12.16 ± 0.61	G	8717.50	11.96 ± 0.60	G
8635.83	11.89 ± 0.24	A	8720.59	13.04 ± 0.26	A
8638.63	12.79 ± 0.50	F, G	8724.56	12.81 ± 0.26	A
8639.84	12.67 ± 0.25	A	8728.55	12.91 ± 0.26	A
8643.72	14.07 ± 0.28	A	8729.38	12.36 ± 0.61	G
8644.56	12.98 ± 0.63	G	8732.56	12.33 ± 0.25	A
8647.76	13.91 ± 0.28	A	8733.36	12.36 ± 0.61	G
8651.67	12.75 ± 0.26	A, G	8736.55	11.64 ± 0.23	A
8653.74	12.30 ± 0.57	F	8742.67	12.21 ± 0.24	B
8655.58	13.19 ± 0.63	G	8743.40	12.24 ± 0.48	F, G
8656.77	13.61 ± 0.27	A	8744.61	12.38 ± 0.50	A
8657.42	13.04 ± 0.71	H	8747.34	12.57 ± 0.62	G
8659.54	13.40 ± 0.64	G	8752.57	12.68 ± 0.25	A
8660.77	13.24 ± 0.26	A	8763.58	12.89 ± 0.52	A
8661.75	13.15 ± 0.82	F	8764.56	12.10 ± 0.24	A
8663.53	12.96 ± 0.50	F, G	8772.63	13.47 ± 0.27	A
8664.77	12.37 ± 0.25	A	8776.56	11.71 ± 0.23	A
8665.77	12.03 ± 0.56	F	8794.57	12.76 ± 0.26	A
8668.81	11.31 ± 0.23	A	8802.25	12.57 ± 0.62	G
8671.52	12.16 ± 0.61	G	8803.27	13.40 ± 0.64	G
8672.72	13.44 ± 0.54	A	8804.47	13.32 ± 0.53	A
8676.71	11.97 ± 0.24	A	8809.54	14.18 ± 0.85	F
8677.80	12.28 ± 0.25	A	8822.48	14.68 ± 0.29	A
8678.68	12.09 ± 0.24	A	8823.22	13.62 ± 0.65	G
8684.52	11.76 ± 0.59	G	8824.47	13.41 ± 0.27	A
8685.80	10.12 ± 0.20	A′	8826.47	14.36 ± 0.29	A
8687.74	9.68 ± 0.19	A″	8830.48	13.32 ± 0.27	A
8688.60	9.92 ± 0.46	G, H	8832.46	14.64 ± 0.29	A
8689.31	10.45 ± 0.88	H	8833.52	14.29 ± 0.85	F

NOTE.—Codes for data origin: A—CTIO spectroscopy; B—OSU spectroscopy; F—OAFA photoelectric photometry; G—SAAO photoelectric photometry; H—VBO CCD photometry.

different from that described by Glass (1992), who found that the amplitude of variation (in magnitudes and flux units) increases with wavelength in the *JHKL* bands.

There is no obvious similarity between the near-IR light curves and the UV and optical ones. However, one should consider that the former are sampled more sparsely, and that we expect them to be smoother than the UV and optical curves because the region which emits the near-IR flux is likely to be much larger than the BLR (Clavel, Wamsteker, & Glass 1989; Glass 1992). Given the limited amplitude and duration of the UV and optical variations, we cannot exclude that corresponding features have simply been smoothed out of the near-IR light curves.

There is no doubt as to the reality of the increase of flux around JD 2,448,780, but the spectral shape of the event is distinctly peculiar. The new *H* and *K* flux observations have been plotted on Figure 2b of Glass (1992), and three of them (JD 2,448,786, JD 2,448,790, and JD 2,448,804, which are also the brightest in *J* and *H*) fall significantly away from the general trend, which is that *H* and *K* are always linearly related. The reality of this interesting behavior must at present be considered provisional. A large number of observers were involved in the work, and small systematic differences between them cannot be entirely excluded.

5. THE LIGHT CURVE OF Hβ

The flux of Hβ was measured as for NGC 5548 in Paper II, by fitting a straight-line continuum in the intervals 4800–4820 Å and 5130–5150 Å, and integrating the flux above the line between 4830 and 4985 Å (Fig. 2). The constant narrow component of Hβ is included in the measurements: its contribution to the total line flux is ∼7 × 10^{-14} erg s^{-1} cm^{-2} (6%–8% of the broad-line flux, depending on the latter's strength).

Winge et al. (1992) have shown that the Hα emission extends to apparent distances of ∼10″ from the nucleus: there is therefore a possibility that the Hβ emission is also extended, and that seeing effects and different slit widths may influence the Hβ fluxes. The internal calibration is not affected, because only the [O III] lines were used for its determination. The broad-line component (which forms the bulk of Hβ) is emitted by an unresolved region, which means that the broad-line fluxes are not affected either. Any extended Hβ emission would only influence the narrow-line component, causing its flux to increase with increasing aperture and seeing. A strong effect is unlikely, since the narrow component is only a small fraction of the measured Hβ flux. The test described in § 3 (the comparison of subsets of quasi-simultaneous Hβ fluxes from CTIO and ESO spectra) yields a negligible offset between the two subsets.

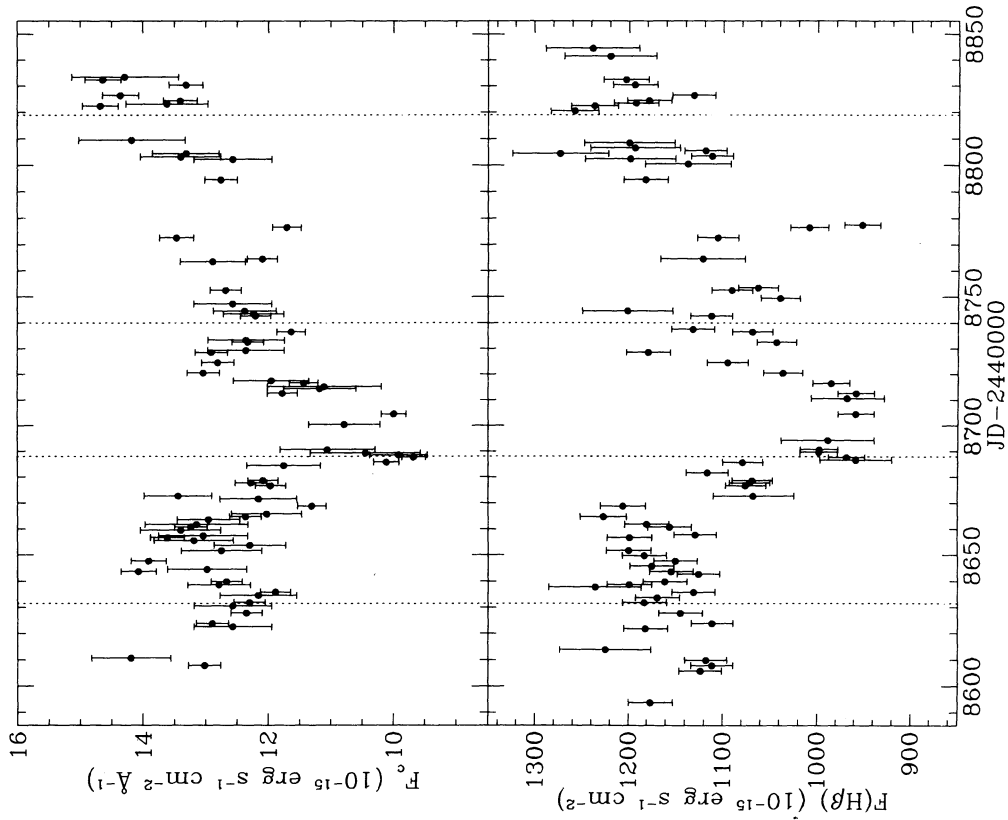Fig. 4.—Light curves of the optical continuum (*top panel*) and of Hβ (*bottom panel*). Dotted vertical lines have been drawn to facilitate comparison with Figs. 8–10 of Paper V.
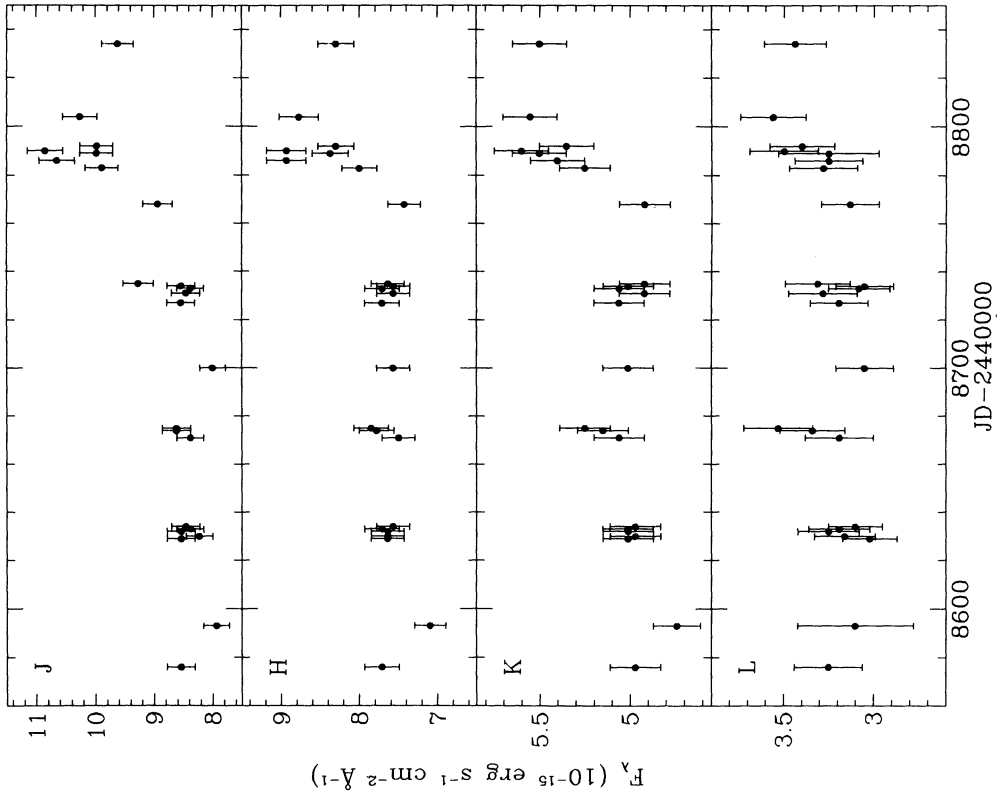
Fig. 5.—Near-IR fluxes obtained at SAAO

TABLE 8

Hβ LIGHT CURVE

JD −2,440,000	$F(H\beta)$ (10^{-15} erg s^{-1} cm^{-2})	Source	JD −2,440,000	$F(H\beta)$ (10^{-15} erg s^{-1} cm^{-2})	Source
8593.83	1176 ± 24	D	8704.58	958 ± 19	A
8605.83	1123 ± 22	D	8710.67	967 ± 39	D
8607.83	1111 ± 22	A	8712.59	958 ± 19	A
8609.81	1118 ± 22	D	8716.60	985 ± 20	A
8613.84	1225 ± 49	D′	8720.59	1036 ± 21	A
8621.83	1182 ± 24	D	8724.56	1095 ± 22	A
8623.83	1111 ± 22	A	8728.55	1179 ± 24	A
8627.83	1144 ± 23	A	8732.56	1042 ± 21	A
8631.84	1183 ± 24	A	8736.55	1068 ± 21	A
8633.81	1169 ± 23	C, D	8737.55	1131 ± 23	D
8635.83	1130 ± 23	A	8742.67	1112 ± 22	B
8637.78	1235 ± 49	C	8744.61	1201 ± 48	A
8638.75	1199 ± 24	C	8749.52	1039 ± 21	D
8639.84	1161 ± 23	A	8752.57	1090 ± 22	A
8642.78	1125 ± 23	C	8753.54	1063 ± 21	D
8643.72	1154 ± 23	A	8764.56	1121 ± 45	A
8645.82	1174 ± 23	D	8772.63	1106 ± 22	A
8647.76	1150 ± 23	A	8776.56	1009 ± 20	A
8649.83	1183 ± 24	D	8777.49	952 ± 19	D
8651.76	1199 ± 24	A	8794.57	1182 ± 24	A
8656.77	1198 ± 24	A	8800.52	1137 ± 45	D
8657.86	1129 ± 23	D	8802.5	1198 ± 48	D
8660.77	1156 ± 23	A	8803.5	1112 ± 22	D
8661.85	1181 ± 24	D	8804.47	1273 ± 51	A
8664.77	1227 ± 25	A	8805.5	1119 ± 22	D
8668.81	1207 ± 24	A	8806.57	1194 ± 48	A
8672.72	1067 ± 43	A	8808.47	1199 ± 48	A
8676.71	1075 ± 22	A	8820.55	1258 ± 25	D
8677.80	1071 ± 21	A	8822.51	1236 ± 25	A, D
8678.68	1068 ± 21	A	8823.50	1193 ± 24	D
8681.71	1117 ± 22	D	8824.50	1178 ± 24	A, D
8685.79	1078 ± 22	A′, D	8826.47	1131 ± 23	A
8686.70	958 ± 38	C	8830.47	1194 ± 24	A
8687.74	968 ± 19	A″	8832.46	1203 ± 24	A
8689.77	998 ± 20	C, D	8841.49	1219 ± 49	D
8690.78	998 ± 20	C	8844.50	1239 ± 50	D
8694.31	988 ± 49	E			

NOTE.—Codes for origin of data as in Table 1.

As the data sets were obtained with different apertures, we conclude that any extended narrow Hβ emission adds a negligible contribution to spectra obtained through large apertures.

The effect of a low resolution on the line flux measurement was simulated by artificially degrading the spectra with the highest resolution, as described in § 3, and repeating the measurement: the Hβ flux always decreased, but never by more than 1%. The 1 σ error bars were estimated as for the continuum fluxes obtained from the spectra (§ 4).

The resulting fluxes and uncertainties are listed in Table 8. Again, fluxes obtained during the same night were averaged. Figure 4 shows the Hβ light curve, in which the median separation between consecutive points is 2.1 days. As for the optical continuum, the similarity to the *IUE* light curves (Paper V) is evident.

6. ANALYSIS OF THE LIGHT CURVES

Inspection of the spectra already reveals that significant variability took place in the optical band. As an example, Figure 6 illustrates how the continuum and broad lines underwent a strong decrease between JD 2,448,661 and JD 2,448,704. Table 9 gives a summary of the main variability characteristics of the optical and IR continua and of Hβ, calculated as in Paper V: the table lists the mean value of each curve

(each point was weighted with the inverse square of its uncertainty), the reduced χ^2 for variability with respect to the mean, and the ratio between the maximum and minimum fluxes, R_{max}. The variability is significant in all light curves except that of the *L*-band flux. The optical continuum varied with a lower amplitude than the UV continua (Paper V), and the multicolor photometry obtained at SAAO, OAFA, and

TABLE 9

VARIABILITY PARAMETERS

Feature	Mean Flux[a]	χ_v^2 [b]	R_{max}[c]
F_λ(opt)	12.4	12.0	1.5 ± 0.1
$F_\lambda(J)$	8.8	10.0	1.4 ± 0.1
$F_\lambda(H)$	7.8	4.2	1.3 ± 0.1
$F_\lambda(K)$	5.1	2.5	1.2 ± 0.1
$F_\lambda(L)$	3.4	0.8	1.2 ± 0.1
$F(H\beta)$	1109	11.2	1.3 ± 0.1

[a] Weighted mean. Units are 10^{-15} erg s^{-1} cm^{-2} Å^{-1} for continuum light curves and 10^{-15} erg s^{-1} cm^{-2} for Hβ light curve.

[b] Reduced χ^2 for variability about mean. Degrees of freedom are 71 for optical continuum, 23 for IR continua, and 72 for Hβ.

[c] Ratio between maximum and minimum values. Uncertainties calculated by propagation of 1 σ flux errors.
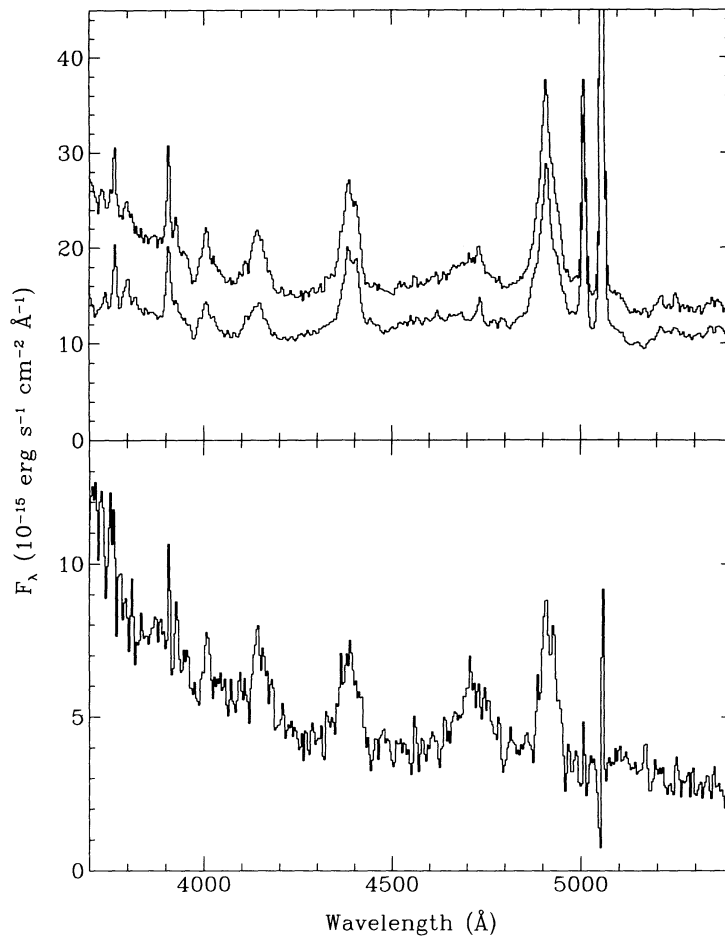
FIG. 6.—*Top panel*: the spectra obtained at CTIO on JD 2,448,660 (*higher curve*) and JD 2,448,704 (*lower curve*). *Bottom panel*: difference between the two spectra shown in the top panel. Notice how the continuum and all the main broad emission lines (particularly He II $\lambda4686$) underwent a strong decrease.

VBO (Tables 2–4) shows that the spectrum is harder when the source is more luminous, confirming the trend displayed by the *IUE* data. This is due at least in part to dilution by the stellar component. Stronger variability has been observed in the past: the U flux varied by 0.38 mag at most during this campaign, while differences in excess of 1.1 mag are present in the U light curve shown by Glass (1992). The variation amplitude of Hβ is lower than that of most UV lines, and comparable to that of C IV $\lambda1549$. If a constant of 7×10^{-14} erg s^{-1} cm^{-2} is subtracted from all Hβ fluxes, in order to correct for the contribution of the narrow component, R_{max} increases slightly to 1.4 ± 0.1.

As already mentioned, a comparison between the light curves in Figure 4 and those presented in Paper V reveals strong similarities. As well as the deep, broad minimum observed in the UV continuum between JD 2,448,680 and JD 2,448,720, most of the secondary minima also have counterparts in the optical curves: those at JD 2,448,631, JD 2,448,668, and JD 2,448,739 are visible in the continuum curve, and those at JD 2,448,668, JD 2,448,728, JD 2,448,739, JD 2,448,767, and JD 2,448,819 can be observed, with a delay, in the light curve of Hβ. Notice that in the Hβ curve the minimum at JD 2,448,767 (delayed to ~JD 2,448,775) is of depth comparable to that of the main minimum, while it is much less pronounced in the UV continuum curves: the two minima have comparable depths also in the light curve of C III] $\lambda1909$ (Paper V).

Unfortunately, most of the period during which the *IUE* was observing at intervals of 2 days instead of 4 days (JD 2,448,783 to JD 2,448,833) was disturbed by bad weather at CTIO and ESO, leading to large gaps and poorer quality in the optical light curves. Thus, while we cannot exclude that the short-timescale "flickering" observed in the UV curves (Paper V) is present also in the optical light curves, the evidence for this is weak.

Figure 7 shows the cross-correlation functions (CCFs) of the optical continuum and Hβ light curves with the F_{1460} continuum curve presented in Paper V. The CCFs were calculated with the method described by Gaskell & Peterson (1987), without artificially extending the light curves beyond their first and last points (in other words, for each lag only the overlapping branches of the curves were cross-correlated). The discrete cross-correlation functions (DCFs) were also calculated as described by Edelson & Krolik (1988), with the differences introduced in Paper V. As Figure 7 shows, the CCFs and DCFs are in good agreement. Notice that each CCF was obtained from light curves which were derived from completely independent data sets: there is therefore no influence on the CCFs by correlated errors as when line and continuum fluxes are obtained from the same spectra (Edelson & Krolik 1988).

The window autocorrelation function (ACF) for the optical continuum (also shown in Fig. 7) was obtained by averaging the ACFs of many white-noise light curves sampled with the
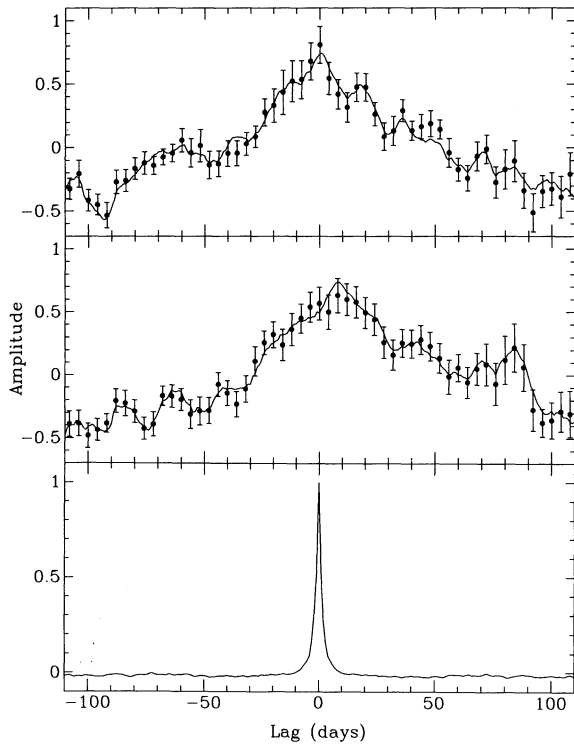
FIG. 7.—*Top panel*: the CCF (*continuous line*) and DCF (*filled circles*) of the F_{1460} continuum curve (Paper V) vs. the optical continuum curve shown in Fig. 4. The DCF is calculated in 4 day bins. *Middle panel*: the CCF and DCF of the F_{1460} continuum curve vs. the Hβ curve shown in Fig. 4. *Bottom panel*: the window ACF for the sampling pattern of the optical continuum. The window ACF for the sampling of the Hβ curve is slightly broader (FWHM = 2.7 days instead of 2.1 days).

same temporal pattern as the continuum curve (Gaskell & Peterson 1987). The full width at half-maximum (FWHM) of the sampling window ACF is 2.2 days, which indicates how much artificial correlation is introduced by interpolating the light curve in order to calculate the CCF. The window ACF for the Hβ light curve is slightly broader (FWHM = 2.7 days). Both window ACFs are much narrower than the CCFs, indicating that the variability on timescales larger than about 2.5 days has been resolved.

The results of the CCF analysis are summarized in Table 10: for each CCF, Δt(peak) is the lag at which it reaches the maximum value, Δt(center) is the average of the two half-maximum lags, and r_{max} is the peak value. Cross-correlating Hβ and the optical continuum with any of the three continuum light curves presented in Paper V yields virtually identical results. How to obtain a reliable uncertainty for the peak lag is still a controversial matter: the method indicated by Gaskell & Peterson (1987) gives an uncertainty of 2 days for all the values of Δt(peak) listed in Table 10. The true uncertainty may be somewhat higher than this but probably does not exceed 4 days.

Notice that the FWHMs of the CCFs are considerably larger than those of the CCFs presented in Paper V. One reason for this is the lower ratio between the amplitude and noise of the variations in the optical light curves. Another possible reason is their less regular sampling. In particular, if the CCFs are calculated without including the points after JD 2,448,777 (thus eliminating the influence of the largest gap in the sampling pattern), the FWHMs of the CCFs become 22.8

TABLE 10
CROSS-CORRELATION RESULTS

Feature	Δt(peak) (days)	Δt(center) (days)	r_{max}	FWHM (days)
Optical continuum versus F_{1460} ⋯	1	1.6	0.741	41.9
Optical continuum versus F_{1835} ⋯	0	1.3	0.746	42.2
Optical continuum versus F_{2700} ⋯	0	2.1	0.760	44.4
F(Hβ) versus F_{1460}	8	7.2	0.737	40.0
F(Hβ) versus F_{1835}	8	7.4	0.742	39.9
F(Hβ) versus F_{2700}	9	19.6	0.684	65.2

days for the optical continuum and 35.3 days for Hβ. Moreover, the main minimum is broader in the Hβ curve than in the continuum curves, and this will naturally broaden the CCF of Hβ. Paper V presented evidence that the variability of NGC 3783 may not be statistically stationary: the irregular sampling of the ground-based campaign could therefore strongly influence the shape of the CCF. The position of the CCF peak, however, is stable. The very large FWHM of the Hβ versus F_{2700} CCF is caused by the fact that its peak is low enough to bring a broad plateau at positive lags just above the half-maximum level.

The optical versus UV continuum CCF reaches its maximum at 0–1 days: as for NGC 5548 (Paper II), therefore, there is no strong evidence that the optical continuum is delayed with respect to the UV continuum. The lag between the light curves of Hβ and F_{1460}, as derived from the peak of the CCF, is ~8 days. This is a factor of 2.5 less than the equivalent result for NGC 5548, and confirms the difference in line versus continuum lags between the two objects, which was evidenced by the *IUE* data (Paper V). Isolating the main minimum in the optical and F_{1460} curves and repeating the cross-correlation yields peak lags of 1 and 6 days for the optical continuum and Hβ, respectively. The last minimum observed in the Hβ curve between JD 2,448,820 and JD 2,448,844, when isolated, yields a lag of 8 days with respect to the corresponding feature of the UV continuum. The difference between lags obtained from isolated minima or from the entire light curves is not significant within the uncertainties discussed above.

Because the near-IR light curves do not show any obvious similarity to the UV and optical curves, we have not used them in the cross-correlation analysis. Glass (1992) found that the near-IR flux followed variations in the optical continuum (U band) at an interval of 80–90 days. While the UV and optical data do not exactly precede the IR by showing a steplike change at the appropriate place, the dip around JD 2,448,700 is followed by an increase which precedes the IR step by about this amount. However, it is unlikely that the two features are related: if they were, one would have to explain the lack of a similar decrease in the IR flux before the brightening and the fact that the rise in flux occurs on comparable timescales (15–20 days) while the emitting regions must be of considerably different sizes.

7. SUMMARY AND CONCLUSIONS

We have presented the results obtained from the ground-based monitoring of the Seyfert 1 galaxy NGC 3783, conducted in 1991–1992 in parallel with the *IUE* monitoring campaign described in Paper V. Light curves of the optical continuum and of Hβ, sampled at median intervals of 2.0 and 2.1 days, respectively, were obtained from spectroscopic and

photometric observations obtained at several observatories. The main results confirm the similarities and differences between NGC 3783 and NGC 5548 evidenced by the *IUE* data, and can be summarized as follows:

1. The optical continuum underwent significant variability, and its light curve strongly resembles that of the UV continuum, with lower amplitude variations.

2. Cross-correlation analysis reveals no observable delay between the variations of the optical and UV continua, within the (possibly conservative) uncertainty of 4 days. This extends to the optical band the trend displayed by the UV continuum light curves (Paper V).

3. A significant increase occurred in the near-IR flux at the end of the campaign, but no feature in the UV/optical continuum curves is an obvious "driver" for it. Considering the width of the K versus U CCF in Glass (1992), it is likely that the UV/optical continuum variations were not intense or long enough for corresponding features, if any are present, to be visible in the near-IR curves.

4. The light curve of Hβ also strongly resembles those of the continua. Cross-correlation analysis reveals that its lag with respect to the UV continuum is about 8 days. As in NGC 5548

(Papers I–III and VII), the light curve of Hβ in NGC 3783 is more delayed with respect to the continuum light curve than those of the high-ionization lines. The lag of Hβ with respect to the continuum is at least twice as long as that of Lyα, about twice that of C IV, and comparable to that of Mg II $\lambda2798$.

5. The Hβ versus continuum lag in NGC 3783 is shorter than in NGC 5548, just as the lags of the high-ionization lines in NGC 3783 are shorter than their counterparts in NGC 5548 (Paper V).

REFERENCES

Alloin, D., et al. 1994, in preparation
Carter, B. S. 1990, MNRAS, 242, 1
Clavel, J., et al. 1991, ApJ, 366, 64 (Paper I)
Clavel, J., Wamsteker, W., & Glass, I. S. 1989, ApJ, 337, 236
de Ruiter, H. R., & Lub, J. 1986, A&AS, 63, 59
Dietrich, M., et al. 1993, ApJ, 408, 416 (Paper IV)
Edelson, R. A., & Krolik, J. H. 1988, ApJ, 333, 646
Evans, I. N. 1988, ApJS, 67, 373
———. 1989, ApJ, 338, 128
Gaskell, C. M., & Peterson, B. M. 1987, ApJS, 65, 1
Glass, I. S. 1992, MNRAS, 256, 23P
Hayes, D. S., & Latham, D. W. 1975, ApJ, 197, 593
Landolt, A. U. 1973, AJ, 78, 959
———. 1983, AJ, 88, 439
Maoz, D., et al. 1993, ApJ, 404, 576
Menzies, J. W., & Feast, M. W. 1983, MNRAS, 203, 1P

Osmer, P., Smith, M., & Weedman, D. W. 1974, ApJ, 189, 187
Pelat, D., Alloin, D., & Fosbury, R. A. E. 1981, MNRAS, 195, 787
Peterson, B. M. 1993, PASP, 105, 247
Peterson, B. M., et al. 1991, ApJ, 368, 119 (Paper II)
Peterson, B. M., et al. 1992, ApJ, 392, 470 (Paper III)
Peterson, B. M., et al. 1994, ApJ, 425, 622 (Paper VII)
Reichert, G. A., et al. 1994, ApJ, 425, 582 (Paper V)
Stirpe, G. M., de Bruyn, A. G., & van Groningen, E. 1988, A&A, 200, 9
van Groningen, E., & Wanders, I. 1992, PASP, 104, 700
Winge, C., Pastoriza, M. G., & Storchi-Bergmann, T. 1990, Rev. Mexicana Astron. Af., 21, 177
Winge, C., Pastoriza, M. G., Storchi-Bergmann, T., & Lipari, S. 1992, ApJ, 393, 98
Winkler, H. 1992, MNRAS, 257, 677
Winkler, H., Glass, I. S., van Wijk, F., Marang, F., Spencer Jones, J. H., Buckley, D. A. H., & Sekiguchi, K. 1992, MNRAS, 257, 659